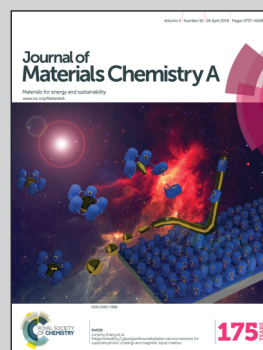


A non-fullerene electron acceptor was developed for polymer solar cells by Dr. Yongxi Li and Prof. Liang-Sheng Liao at the Institute of Functional Nano & Soft Materials (FUNSOM), Soochow University.

Title: Non-fullerene acceptor with low energy loss and high external quantum efficiency: towards high performance polymer solar cells

A non-fullerene electron acceptor bearing a fused 10-heterocyclic ring (indacenodithiopheno-indacenodithiophene) with narrow band gap (~ 1.5 eV) was designed and synthesized. When this acceptor was applied in polymer solar cells, a power conversion efficiency of 6.5% was achieved with an energy loss as low as 0.59 eV.

As featured in:



See Yi Zhou, Zuo-Quan Jiang, Feng Gao, Liang-Sheng Liao *et al.*, *J. Mater. Chem. A*, 2016, 4, 5890.



www.rsc.org/MaterialsA

Registered charity number: 207890

CrossMark
click for updatesCite this: *J. Mater. Chem. A*, 2016, 4, 5890

Non-fullerene acceptor with low energy loss and high external quantum efficiency: towards high performance polymer solar cells†

Yongxi Li,^{‡a} Xiaodong Liu,^{‡b} Fu-Peng Wu,^a Yi Zhou,^{*b} Zuo-Quan Jiang,^{*a} Bo Song,^b Yuxin Xia,^c Zhi-Guo Zhang,^d Feng Gao,^{*c} Olle Inganäs,^c Yongfang Li^{bd} and Liang-Sheng Liao^{*a}

A non-fullerene electron acceptor bearing a fused 10-heterocyclic ring (indacenodithiopheno-indacenodithiophene) with a narrow band gap (~1.5 eV) was designed and synthesized. It possesses excellent planarity and enhanced effective conjugation length compared to previously reported fused-ring electron acceptors. When this acceptor was paired with PTB7-Th and applied in polymer solar cells, a power conversion efficiency of 6.5% was achieved with a high open circuit voltage of 0.94 V. More significantly, an energy loss as low as 0.59 eV and an external quantum efficiency as high as 63% were obtained simultaneously.

Received 22nd January 2016
Accepted 17th February 2016

DOI: 10.1039/c6ta00612d

www.rsc.org/MaterialsA

1. Introduction

Polymer solar cells (PSCs) have experienced rapid progress during past decades. The power conversion efficiency (PCE) has reached as high as 10.8% for a single bulk heterojunction (BHJ) cell.¹ In terms of the theoretical maximum PCE, there is still much room to improve. One of the main limitations is the lack of high performance narrow-bandgap absorbers ($E_g < 1.6$ eV) with both high open circuit voltage (V_{oc}) and high external quantum efficiency (EQE) at the same time.² One solution to maximize the V_{oc} is to reduce the energy loss (E_{loss}) happening during the dissociation of excitons and the generation of free charge carriers. A small E_{loss} often promises an additional increase of V_{oc} .³

For solar cells, E_{loss} can be caused by either radiative or non-radiative recombination of charge carriers. The non-radiative loss in PSCs is usually very high (larger than 300 meV) as a result of low emission efficiency.⁴ For the radiative loss, part of it is unavoidable, which is depicted as the Shockley–Queisser (SQ)

limit.⁵ Detailed balance principle requires that the photo absorbers should also emit light as they generate electrons. This loss is typically 250 meV in the majority of solar cells. On top of that, PSCs usually demonstrate additional radiative loss due to absorption below the bandgap, also known as the absorption from the charge-transfer (CT) states. The CT state absorption usually extends towards much lower energies compared with the onset of absorption of the pure components.⁶ For most fullerene-based PSCs, this additional loss is larger than 200 meV, which is one of the main reasons why the PCSs with the highest performance in the literature have E_{loss} values ranging from 0.7 to 0.8 eV, much bigger than that of highly efficient perovskite solar cells, whose values are commonly below 0.5 eV.⁷

Non-fullerene acceptor-based PSCs are nowadays experiencing rapid development.⁸ Due to their versatile molecular structure, adjustable energy levels and tunable charge mobility, the small conjugated molecules supply a large library for the acceptors. In general, the trade-off feature of E_{loss} and high EQE exists in PSCs based on fullerene, as well as non-fullerene acceptors.³ However, the molecular variety of non-fullerene acceptors may render the possibility of matching the narrow-band-gap donors so that there would be no trade-off feature, resulting in improved high performance. In this regard, only a few cases have been demonstrated in the literature, mainly due to the fact that the development of acceptor materials lags far behind the rapid advances in polymer donors.

As an alternative to fullerenes, multi fused-ring ladder-type conjugated molecules show great potential, as rigid coplanar structures can efficiently restrain rotational disorder.^{8j,k,9} In this article, we present a non-fullerene-based electron acceptor bearing a fused 10-heterocyclic ring (indacenodithiopheno-indacenodithiophene), denoted by **IDTIDT-IC**. This molecule

^aJiangsu Key Laboratory for Carbon-Based Functional Materials & Devices, Institute of Functional Nano & Soft Materials (FUNSOM), Soochow University, Suzhou, Jiangsu, 215123, P. R. China. E-mail: zqjiang@suda.edu.cn

^bLaboratory of Advanced Optoelectronic Materials, College of Chemistry, Chemical Engineering and Materials Science, Soochow University, Suzhou, Jiangsu 215123, P. R. China. E-mail: yizhou@suda.edu.cn

^cBiomolecular and Organic Electronics, IFM, Linköping University, Linköping 58183, Sweden. E-mail: fenga@ifm.liu.se

^dBeijing National Laboratory for Molecular Sciences, Institute of Chemistry, Chinese Academy of Sciences, Beijing 100190, China

† Electronic supplementary information (ESI) available. See DOI: 10.1039/c6ta00612d

‡ Dr Yongxi Li and Dr Xiaodong Liu contributed equally to this work.

can simultaneously broaden the absorption ($\lambda_{\text{edg}} \sim 810$ nm) and increase the level of its LUMO. This will in turn improve both the short current density (J_{sc}) and the open circuit voltage (V_{oc}) in devices. More interestingly, as this molecule was paired with PTB7-Th, an E_{loss} as low as 0.59 eV and an EQE as high as 63% were obtained. Without any additive, PSCs based on this photoactive pairing showed a maximum PCE of up to *ca.* 6.5% with a V_{oc} of 0.94 V.

2. Results and discussion

The molecular structure of **IDTIDT-IC** is shown in Scheme 1. The large conjugate plane of **IDTIDT-IC** allows for low reorganization energy, more wavefunction delocalization and a narrow band gap. The alkyl-chain substitutions were designed to increase the solubility of **IDTIDT-IC** and alleviate the aggregation of molecules through spatial hindrance. The 3-(dicyanomethylidene)indan-1-one moieties terminated at both sides have a strong electron withdrawing effect, and were expected to possess good n-type transport properties. In order to investigate the effect of conjugation length on the optoelectronic characteristics, an analogous molecule bearing a fused 5-heterocyclic ring was synthesized as reference, and denoted by **IDT-IC** (Scheme 1). These two materials acted as acceptors and were paired with PTB7-Th in BHJ PSCs.

As shown in Fig. 1a, both **IDT-IC** and **IDTIDT-IC** exhibit two strong absorption bands, with a shorter wavelength band due to π - π^* transitions, and a longer wavelength band due to intramolecular charge transfer (ICT). The absorption peaks of **IDT-IC** and **IDTIDT-IC** in chloroform are located around 646 and 696 nm. It is not hard to understand that elongation of the conjugation length results in a reduced band-gap (E_{g}).⁹ In the film state, the absorption bands of **IDT-IC** and **IDTIDT-IC** (Fig. 1b) both shift to longer wavelengths, which can be explained by the formation of J-aggregates between the big aromatic moieties. The E_{g} values extracted from their absorption band edges are 1.72 and 1.53 eV for **IDT-IC** and **IDTIDT-IC**, respectively. The energy levels of the two acceptors were determined using cyclic voltammetry (CV) with ferrocene as reference. The current density–voltage (J - V) curves are shown in Fig. 1c. The highest

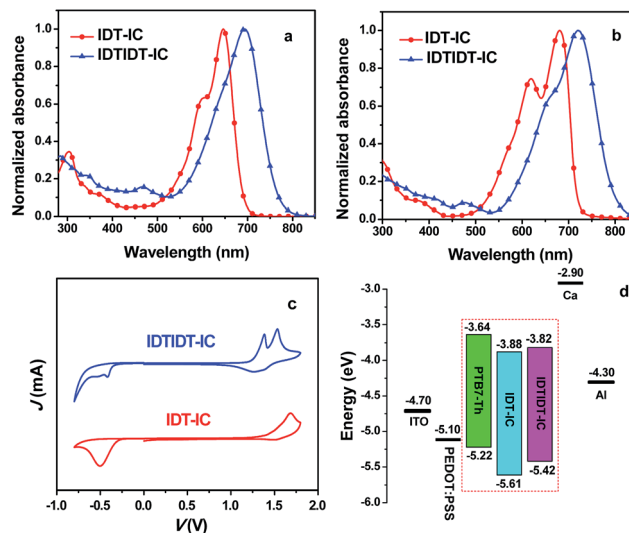
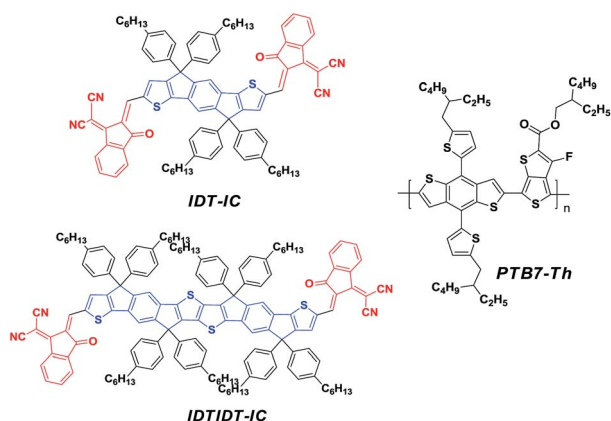


Fig. 1 The normalized UV-vis spectra of **IDT-IC** and **IDTIDT-IC** (a) in chloroform and (b) in the film state; (c) the CV curves of **IDT-IC** and **IDTIDT-IC** in $\text{CH}_3\text{CN}/0.1 \text{ M } [\text{nBu}_4\text{N}]^+[\text{PF}_6]^-$ at 100 mV s^{-1} , the horizontal scale refers to the Ag/AgCl electrode; (d) energy diagram relative to the vacuum level.

occupied molecular orbital (HOMO) and the lowest unoccupied molecular orbital (LUMO) levels were deduced from the onset of the oxidation and reduction peaks, and the results are summarized in Table 1. The HOMO/LUMO levels of **IDT-IC** and **IDTIDT-IC** were $-5.61/-3.88$ eV and $-5.42/-3.82$ eV, respectively. Fig. 1d shows the energy diagram relative to the vacuum level. Interestingly, for these two acceptors, the elongation of conjugation length causes the elevation of the energy levels, especially the LUMO levels. It can be speculated from the LUMO levels that **IDTIDT-IC** should lead to a relatively higher V_{oc} when used in PSCs. This result indicated that the enhancement of the conjugation length of the multi-fused acceptor could not only be advantageous to achieve better absorption of solar photon flux, but also be beneficial for achieving higher V_{oc} of PSCs using it as an acceptor.

In order to gain a deeper insight on the geometric and electronic properties of these acceptor molecules, density functional theory (DFT) calculations were performed at the B3LYP/6-31G (d) level. From Fig. 2, we can clearly see that the HOMO/LUMO wavefunctions of both molecules are well delocalized over the backbone. This high degree of HOMO/LUMO delocalization is contributed by the highly coplanar backbones. Meanwhile, the optimized geometries are also investigated. Both **IDTIDT-IC** and **IDT-IC** show quite planar structures with extremely small torsion angles (**IDTIDT-IC** = 0.15° , **IDT-IC** = 0.35°). This highly planar geometry would facilitate π -electron delocalization and enhance charge mobility. In addition, the aryl side-chains are outside of the backbones, which suppress the strong aggregation of fused aromatic rings, and also form a 3D conformation.

The fluorescence spectra of pure PTB7-Th, **IDT-IC**, **IDTIDT-IC** and an optimized blend film of PTB7-Th with **IDT-IC** or **IDTIDT-IC** are shown in Fig. 3a and b. The PL intensity is



Scheme 1 Chemical structures of **IDTIDT-IC**, **IDT-IC** and PTB7-Th.

Table 1 Optical and electrochemical properties of non-fullerene acceptors IDT-IC and IDTIDT-IC

Acceptors	UV-vis absorption					Cyclic voltammetry		
	Solution		Film		Bandgap/eV	HOMO/eV	LUMO/eV	Bandgap/eV
	λ_{\max}/nm	$\lambda_{\text{onset}}/\text{nm}$	λ_{\max}/nm	$\lambda_{\text{onset}}/\text{nm}$				
IDT-IC	646	692	681	720	1.72	-5.61	-3.88	1.73
IDTIDT-IC	696	771	721	810	1.53	-5.42	-3.82	1.60

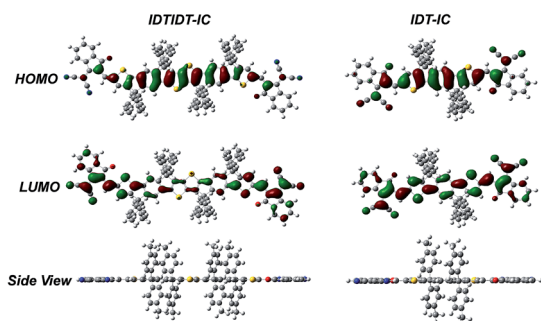


Fig. 2 Molecular geometries and HOMO/LUMO wavefunctions of the dimer models of IDTIDT-IC and IDT-IC.

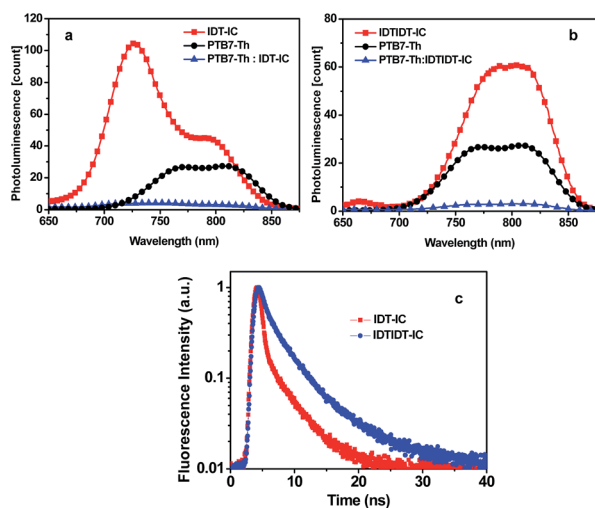


Fig. 3 (a) Photoluminescence spectra of PTB7-Th (excitation at 600 nm), PTB7-Th : IDT-IC (1 : 1.5, w/w) (excitation at 600 nm) and IDT-IC (excitation at 600 nm) in the thin film; (b) photoluminescence spectra of PTB7-Th (excitation at 600 nm), PTB7-Th : IDTIDT-IC (1 : 1.5, w/w) (excitation at 620 nm) and IDTIDT-IC (excitation at 620 nm) in the thin film and (c) time-resolved fluorescence of IDT-IC and IDTIDT-IC in chloroform solution (the concentration for each is about 0.1 mmol L⁻¹).

quenched by a factor of 20.6 in the PTB7-Th/IDT-IC and a factor of 22.7 in the PTB7-Th/IDTIDT-IC blended films. Given that nearly all the excitons in the polymer phases are created close enough to an interface, they are quenched in both of the blended films. In order to investigate the radiative/non-radiative recombination processes in the excited state of non-

fullerene electron acceptor materials, time-resolved fluorescence spectra of IDT-IC and IDTIDT-IC were measured. The fluorescence decay of IDT-IC is much faster than that of IDTIDT-IC as shown in Fig. 3c. The fitted decay lifetime from the time-resolved PL data are 1.1 and 3.1 ns for IDT-IC and IDTIDT-IC, respectively. The enhanced effective conjugated length of IDTIDT-IC and its lower degree of rotational freedom causes the longer PL lifetime.⁹ Considering this, the charge-carrier diffusion length is relative to the PL lifetime quenching ratios.¹⁰ The longer lifetime of the excited state in IDTIDT-IC should facilitate excitons to diffuse to the donor-acceptor interface more efficiently for photocurrent generation.

When utilizing non-fullerene acceptor materials for PSCs, high electron mobility is very critical to obtain high performance devices, since it is directly related to charge transport and recombination. In order to probe how the conjugated length of the molecules influences electron transport within these non-fullerene materials, their electron mobilities were measured by the space charge limited current (SCLC) method using electron-only devices with the structure ITO/Cs₂CO₃/PTB7-Th : acceptor/Ca/Al at the optimized blend ratio. As shown in Fig. S2 and Table S3 in ESI,[†] the electron mobilities of PTB7-Th:IDT-IC and PTB7-Th:IDTIDT-IC are estimated as 2.09 × 10⁻⁵ and 4.54 × 10⁻⁵ cm² V⁻¹ s⁻¹ respectively, at a typical electric field of 10⁷ V m⁻¹. The electron mobility of IDTIDT-IC is twice as high than that of IDT-IC. This improvement in electron mobility can be ascribed to enhanced orbital overlap and decreased reorganization energy of IDTIDT-IC.⁹ As a result, high values of J_{sc} and FF can thus be expected.

Using IDT-IC and IDTIDT-IC as acceptors, BHJ PSCs with the device configuration of ITO/PEDOT:PSS/PTB7-Th:acceptor/PDINO/Al were fabricated and characterized, where PDINO is a cathode buffer layer.¹¹ The details of the fabrication and optimization of devices, such as donor/acceptor blend ratio, thickness of the photoactive layer and interfacial engineering, are presented in the ESI.[†] The J - V curves evaluated under illumination of air mass 1.5 Global (AM 1.5G) are shown in Fig. 4. The photovoltaic parameters of these devices are summarized in Table 2. For both of these two acceptors, the optimized donor/acceptor ratio was 1/1.5. The devices with IDT-IC as acceptor showed a highest PCE value of 3.16% with V_{oc} , short current density (J_{sc}) and fill factor (FF) of 0.83 V, 9.53 mA cm⁻² and 40.0%, respectively. The device based on IDTIDT-IC reached a summit PCE value of 6.48% with V_{oc} , J_{sc} and FF of 0.94 V, 14.49 mA cm⁻² and 47.5%, respectively. It is worth noting that no additives were involved in the photoactive blends. The

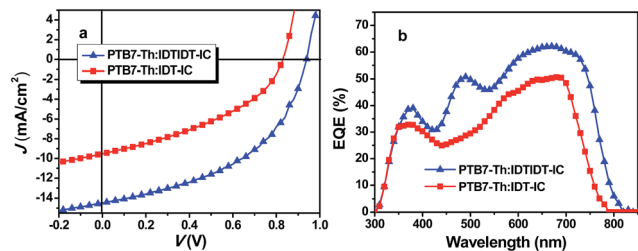


Fig. 4 (a) The J - V characteristics and (b) EQE spectra of the PSCs based on PTB7-Th:IDT-DT-IC and PTB7-Th:IDT-IC (blend ratio of 1:1.5, w/w) with PDINO as a cathode interlayer.

Table 2 Photovoltaic parameters of the PSCs based on PTB7-Th as donor and IDT-IC, IDT-DT-IC or PC₇₁BM as acceptors under the illumination of AM 1.5G, 100 mW cm⁻²

Acceptors	V_{oc} (V)	J_{sc} (mA cm ⁻²)	FF (%)	PCE _{max} (%)	PCE _{ave} ^a (%)
IDT-IC	0.83	9.53	40.0	3.16	3.05 ± 0.10
IDT-DT-IC	0.94	14.49	47.5	6.48	6.25 ± 0.14
PC ₇₁ BM	0.76	16.37	59.6	7.43	7.12 ± 0.18

^a Average values obtained from five devices with standard deviation.

corresponding EQE curves of the above devices are presented in Fig. 4b. The cut-off values of IDT-IC and IDT-DT-IC at the longer wavelength side were 780 and 810 nm, respectively. Besides, the EQE signals of the latter were much higher throughout the 400–810 nm range, especially in the range of 450–550 nm, which correspond well to the additional π - π^* transition absorption of IDT-DT-IC (Fig. 1a and b). Clearly, IDT-DT-IC shows a relatively high potential when being applied as acceptor material. The higher photocurrent generation can be ascribed to the enhanced light absorption of IDT-DT-IC caused by the elongation of the conjugation length.

As shown above, the V_{oc} (0.94 V) for the device based on PTB7-Th:IDT-DT-IC was surprisingly high even with such narrow E_g (~1.5 eV). To highlight this feature, we summarized a series of eV_{oc} vs. E_g for PSCs with reported PCE > 5% in the literature^{8,12} (Fig. 5a). Included in the plot is a red line corresponding to $E_g - eV_{oc} = 0.6$ eV. This value is often used as an approximation to the maximum voltage for a specific BHJ blend. To date, most devices are located below the red line. For

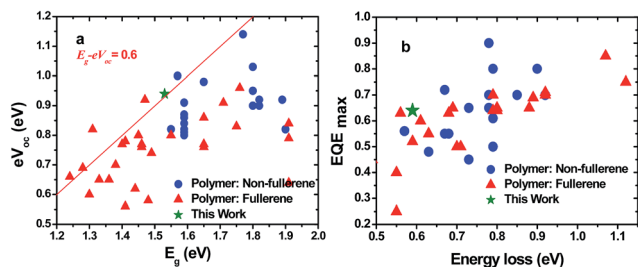


Fig. 5 (a) E_g vs. V_{oc} distributions of recent high performance PSCs based on low E_g polymers. (b) Plot of maximum EQE vs. E_{loss} .

devices based on non-fullerene acceptors, all of them are far below the line. Herein, the devices based on PTB7-Th:IDT-DT-IC stay right on the line. This result means that the V_{oc} obtained is already very high based on the E_g (obtained from the UV-vis spectra) of the acceptors.

Generally, the energy difference between the HOMO of the donor and the LUMO of the acceptor is empirically used to predict the V_{oc} in BHJ PSCs. The E_{loss} defined by $E_{loss} = E_g - qV_{oc}$ is also an important parameter to interpret the deviation of V_{oc} . Note E_g is determined by the smaller value of donor or acceptor materials. Herein E_g refers to the E_g value of IDT-DT-IC which has a relatively smaller value. Fig. 5b plots the E_{loss} vs. the corresponding maximum EQE for PSCs in the literature.^{8,12} These two factors often show a trade-off feature. In the published cases, few donor/acceptor pairs can generate a low E_{loss} and a high EQE at the same time. Most of the polymer blends show an E_{loss} of more than 0.7 eV. And when the E_{loss} is at the 0.7 eV level, the corresponding EQE dropped to less than 60%. In our case, the E_{loss} was as low as 0.59 eV for PTB7-Th:IDT-DT-IC, which as we know is the lowest value among the PSCs using non-fullerene as acceptors. More importantly, an EQE as high as 63% was at the same time retained. These results indicate that the non-fullerene acceptor material is able to couple with narrow E_g polymers and achieve a quite low E_{loss} value and maintain a high EQE.

To investigate the contribution of exciton dissociation and charge extraction to such a high EQE, an internal quantum efficiency (IQE) spectrum was calculated based on the total absorption spectrum and the EQE of the PTB7-Th:IDT-DT-IC solar cell with a PDINO cathode interlayer. As shown in Fig. S6,[†] the IQE of the PTB7-Th:IDT-DT-IC solar cell approaches 100% at ca. 520 nm and remains near or even above 80% throughout nearly the entire absorption spectrum (410–770 nm). Such high IQE values indicate that almost every absorbed photon is converted to a separated pair of charge carriers and that almost all photogenerated carriers are collected at the electrodes.

To get insight into the high V_{oc} (*i.e.* quite low E_{loss}), Fourier-transform photocurrent spectroscopy (FTPS) was performed. For BHJ PSCs, V_{oc} is correlated to the energy of the charge transfer (E_{CT}) state formed at the donor/acceptor interface.⁶ A high V_{oc} requires a high E_{CT} which can be maximized by a relatively small CT state energy loss (ΔE).¹³ The relationship between E_{CT} and E_g can be expressed by the equation: $E_{CT} = E_g - \Delta E$.

The FTPS for the solar cells based on PTB7-Th, PTB7-Th:PC₇₁BM and PTB7-Th:IDT-DT-IC are shown in Fig. 6a. The absorption of the PTB7-Th:IDT-DT-IC blend almost overlaps with that of pure PTB7-Th, and there is no additional absorption below the bandgap. Therefore, no obvious CT absorption was observed in the spectrum. This result suggests that the radiative recombination loss is rather small at the CT state. The overlapping of FTPS spectra of PTB7-Th and PTB7-Th:IDT-DT-IC also means that the driving force for CT between the donor and acceptor is rather small. In other words, the E_{CT} is large enough to generate a high V_{oc} . On the contrary, the FTPS spectrum of the PTB7-Th:PC₇₁BM blend shows a strong and clear absorption from the CT state indicated by the fitted curve.

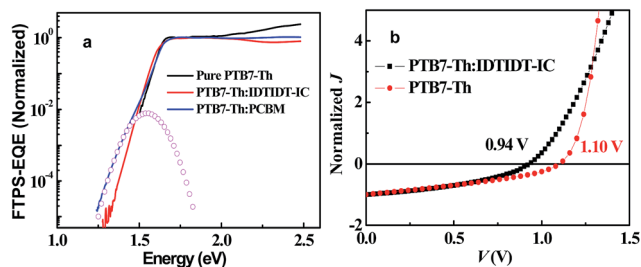


Fig. 6 (a) FTPS spectra of the polymer donor PTB7-Th, PTB7-Th:IDTIDT-IC and PTB7-Th:PCBM blend. (b) The J - V characteristics of the PSCs based on PTB7-Th:IDTIDT-IC and PTB7-Th.

This CT state absorption enhances the radiative loss and hence decreases the V_{oc} in the corresponding devices. This explains the relatively high V_{oc} of 0.94 V for the device based on PTB7-Th:IDTIDT-IC versus 0.78 V for devices based on PTB7-Th:PC₇₁BM.

In addition to the radiative loss, the non-radiative loss in organic solar cells is usually very high and causes low emission efficiency.⁴ The V_{oc} loss caused by non-radiative recombination can be calculated based on eqn (1), where EQE_{EL} is the electroluminescence quantum efficiency of the solar cells (measured in darkness under the forward bias). The EQE_{EL} of the PTB7-Th:IDTIDT-IC blend and pure PTB7-Th were 2×10^{-6} and 5×10^{-4} , corresponding to V_{oc} losses of 0.34 and 0.20 V, respectively. The non-radiative loss difference was 0.14 V. Since the CT absorption was not observed in the FTPS spectra, we assume that the radiative loss for the devices based on PTB7-Th and PTB7-Th:IDTIDT-IC should be similar. Thus, the V_{oc} difference between these two devices can be attributed to the difference of non-radiative recombination, *i.e.* 0.14 V. This value agrees well with the V_{oc} difference of 0.16 V between these two devices, as shown in Fig. 6b. These results indicate that a high EQE can be maintained with a negligible driving force.

$$\Delta V_{oc}^{non-rad} = -\frac{kT}{q} \ln(EQE_{EL}) \quad (1)$$

Another possible reason for obtaining high V_{oc} is that the larger conjugation length of IDTIDT-IC decreases the exciton binding energy of charges in the CT state.¹⁴ This assumption is consistent with the results reported by Friend *et al.*¹⁵ They demonstrated that structural rigidity and suppressed torsion relaxation will result in more extended wavefunctions and low reorganization energies, and this will decrease the barrier for formation of polarons and allow for efficient charge separation with minimal band offsets. As a consequence, the V_{oc} as well as PCE can be greatly improved.

3. Conclusions

In summary, two fused-ring ladder-type non-fullerene acceptors have been designed and synthesized. Due to the enhancement of effective conjugation length, the acceptor shows a lower band-gap, better planarity and a higher LUMO level. When

using IDTIDT-IC which has longer conjugated length as acceptor, we have realized very low E_{loss} (<0.6 eV) and high EQE (>60%) values, and as a consequence, a superior PCE of up to 6.5%. Without any additives, the V_{oc} of the devices reached 0.94 V, which is surprisingly high compared to the often reported 0.76 V for devices based on PTB7-Th:PC₇₁BM. The high V_{oc} can be attributed to the very low E_{loss} of the donor/acceptor pair. This work demonstrated the great potential of a non-fullerene acceptor in coupling with narrow-band-gap polymers for high performance PSCs.

4. Experimental

Materials and characterization

All chemicals, unless otherwise specified, were purchased from TCI and used as received. IDT was synthesized according to the reported procedure.¹⁶ UV-vis spectra were measured using a Perkin-Elmer Lambda-9 spectrophotometer. The ¹H and ¹³C NMR spectra were collected on a Bruker AV400 and 500 spectrometer operating at 400 and 125 MHz in deuterated chloroform solution with TMS as reference, respectively. Time of Flight MS-MALDI (TOF) MS were performed on a Bruker Autoflex II/Compass 1.0 from Soochow University, Department of Materials Science and Engineering. MS spectra were recorded on Bruker Esquire LC-Ion Trap. Cyclic voltammetry of polymer film was conducted in acetonitrile with 0.1 M of tetrabutylammonium hexafluorophosphate using a scan rate of 100 mV s⁻¹. ITO, Ag/AgCl and Pt mesh were used as the working electrode, reference electrode and counter electrode, respectively. The steady-state photoluminescence spectra and time resolved photoluminescence were measured by utilizing Horiba Jobin-Yvon Lab RAM HR800 and a single photon counting spectrometer, which was combined with the Fluorolog-3 spectrofluorometer (Horiba-FM-2015), respectively. A 300 nm laser source was used in the time resolved PL measurement.

Synthesis methods

Synthesis of compound 1. To a stirred solution of thieno[3,2-*b*]thiophene (420 mg, 3.0 mmol) in dry THF (20 mL) was added dropwise a 2.4 M solution of *n*-butyllithium in hexane (2.7 mL, 6.5 mmol) at -78 °C under argon atmosphere. After being stirred for 30 min at -78 °C, the resulting solution was warmed to room temperature and stirred for another 30 min. Then anhydrous zinc chloride (1.3 g, 10.0 mmol) in dry THF (100 mL) was added to the mixture dropwise. The mixture was stirred for 1 h at 0 °C, which was then increased to room temperature. Diethyl 2,5-dibromoterephthalate (2.5 g, 6.5 mmol) and Pd(PPh₃)₄ (140 mg, 0.12 mmol) were added directly. The reaction mixture was refluxed overnight. Upon completion, the reaction mixture was filtered over celite, extracted with ethyl acetate and then dried over anhydrous Na₂SO₄. The product was purified by silica gel chromatography to afford a light yellow solid (0.75 g, 32%). ¹H NMR (400 MHz, CDCl₃, δ): 8.03 (s, 2H), 7.91 (s, 2H), 7.24 (s, 2H), 4.46 (q, *J* = 8.0 Hz, 4H), 4.28 (q, *J* = 8.0 Hz, 4H), 1.44 (t, *J* = 8.0 Hz, 6H), 1.20 (t, *J* = 8.0 Hz, 6H). ¹³C NMR (125 MHz, CDCl₃, δ): 166.3, 165.2, 141.6, 139.9, 136.8, 135.2,

134.1, 133.6, 133.1, 121.2, 119.4, 62.3, 62.1, 14.2, 13.9. MS-ESI ($M + H$)⁺ calcd for C₃₀H₂₆Br₂O₈S₂, 737.9; found, 737.9.

Synthesis of compound 2. The compound 1 (738 mg, 1.0 mmol) was dissolved in toluene (50 mL) and the tributyltin thiophene (1.1 g, 3.0 mmol) was then added. The mixture was deoxygenated by bubbling nitrogen gas through it for 30 minutes and then Pd(PPh₃)₄ (46 mg, 4 mol%) was added. The mixture was refluxed for 24 h under the nitrogen atmosphere and then cooled to room temperature. The solvent was evaporated and the crude product was purified with silica gel chromatography using 5 : 1 (DCM : hexane) as the eluent. Evaporation of the solvent yielded the product as a yellow solid (684 mg, 92%). ¹H NMR (400 MHz, CDCl₃, δ): 7.88 (s, 2H), 7.85 (s, 2H), 7.41 (d, *J* = 4.0 Hz, 2H), 7.29 (s, 2H), 7.11 (m, 4H), 4.27 (m, 8H), 1.19 (t, *J* = 8.0 Hz, 12H). ¹³C NMR (125 MHz, CDCl₃, δ): 167.1, 167.0, 141.7, 139.8, 139.4, 133.7, 133.5, 133.4, 132.8, 131.6, 131.5, 126.9, 126.6, 126.1, 61.3, 61.2, 13.4, 13.3. MS-ESI ($M + H$)⁺ calcd for C₃₈H₃₂O₈S₄, 744.1; found, 744.1.

Synthesis of IDTIDT. 1-Bromo-4-hexylbenzene (1.6 g, 6.7 mmol) was dissolved in THF (50 mL) and placed under a nitrogen atmosphere. The solution was cooled to −78 °C and stirred while 2.4 M *n*-butyllithium in hexane (2.8 mL, 6.7 mmol) was added dropwise. The mixture was stirred for 1 h at −78 °C, and then a solution of 2 (500 mg, 0.67 mmol) in THF (25 mL) was added dropwise. The reaction was warmed to room temperature and stirred overnight, and then poured into water and extracted with dichloromethane (3 × 50 mL). The organic extracts were combined and dried over anhydrous Na₂SO₄. After removal of the solvent, the crude product was charged into a three-neck flask. Acetic acid (50 mL) and concentrated H₂SO₄ (1.0 mL) were added and the mixture was refluxed for 2 h. Then the mixture was poured into water and extracted with hexane. The resulting crude compound was purified by silica gel chromatography using a mixture of hexane/DCM as the eluent to give a light yellow solid (710 mg, 60%). ¹H NMR (400 MHz, CDCl₃, δ): 7.46 (s, 2H), 7.31 (s, 2H), 7.23 (d, *J* = 4.0 Hz, 2H), 7.18 (m, 16H), 7.08 (m, 16H), 6.99 (d, *J* = 4.0 Hz, 2H), 2.56 (t, *J* = 8.0 Hz, 16H), 1.60–1.53 (m, 16H), 1.35–1.29 (m, 48H), 0.86 (t, *J* = 4.0 Hz, 24H). ¹³C NMR (125 MHz, CDCl₃, δ): 155.9, 153.7, 152.9, 146.7, 142.8, 141.8, 141.3, 140.5, 135.7, 135.2, 128.4, 128.3, 128.1, 128.0, 127.8, 127.5, 123.1, 117.1, 62.9, 62.7, 35.6, 31.7, 31.4, 31.2, 29.3, 29.2, 22.6, 14.2. HRMS (MALDI) *m/z*: M⁺, calcd for C₁₂₆H₁₄₄S₄, 1786.0184; found, 1785.520.

Synthesis of IDTIDT-CHO. In a dry round-bottomed flask, compound IDTIDT (470 mg, 0.27 mmol) was dissolved in THF (50 mL) and placed under a nitrogen atmosphere. The solution was cooled to −78 °C and stirred while 2.4 M *n*-butyllithium in hexane (0.29 mL, 0.68 mmol) was added dropwise. The mixture was stirred for one hour at −78 °C, and then anhydrous DMF (79 mg, 1.08 mmol) was added dropwise. The reactant was warmed to room temperature and stirred overnight. Thereafter, brine was added and extracted with DCM. The resulting crude compound was purified by silica gel chromatography using a mixture of hexane/DCM as the eluent to give a yellow solid (353 mg, 71%). ¹H NMR (400 MHz, CDCl₃, δ): 9.79 (s, 2H), 7.63 (s, 2H), 7.58 (s, 2H), 7.35 (s, 2H), 7.18 (m, 16H), 7.09 (m, 16H), 2.55 (t, *J* = 8.0 Hz, 16H), 1.60–1.53 (m, 16H), 1.35–1.29 (m, 48H),

0.86 (t, *J* = 4.0 Hz, 24H). ¹³C NMR (125 MHz, CDCl₃, δ): 182.3, 155.6, 154.6, 153.3, 147.5, 144.9, 142.5, 141.6, 141.5, 140.4, 139.4, 137.4, 128.6, 128.1, 127.8, 127.5, 127.1, 124.8, 62.5, 62.3, 35.1, 31.2, 30.9, 30.7, 28.6, 22.1, 13.7. HRMS (MALDI) *m/z*: M⁺, calcd for C₁₂₈H₁₄₄O₂S₄, 1842.0083; found, 1841.262.

Synthesis of IDTIDT-IC. 1,1-Dicyanamethylene-3-indanone (194 mg, 1.0 mmol) was added into the mixture of compound IDTIDT-CHO (170 mg, 0.1 mmol) in chloroform with pyridine (1 mL). The reactant was deoxygenated with nitrogen for 30 min and then reflux for 10 h. After cooling to room temperature, the reactant was poured into methanol and the precipitate was filtered off, then extracted with DCM and washed with water. The crude product was purified by silica gel using a mixture of hexane/DCM as the eluent to give a purple solid (171 mg, 78%). ¹H NMR (400 MHz, CDCl₃, δ): 8.87 (s, 2H), 8.68 (d, *J* = 8.0 Hz, 2H), 7.90 (d, *J* = 8.0 Hz, 2H), 7.67 (m, 8H), 7.37 (s, 2H), 7.14 (m, 32H), 2.56 (t, *J* = 8.0 Hz, 16H), 1.60–1.53 (m, 16H), 1.35–1.29 (m, 48H), 0.86 (t, *J* = 4.0 Hz, 24H). ¹³C NMR (125 MHz, CDCl₃, δ): 188.5, 160.8, 160.5, 157.2, 156.5, 154.2, 148.7, 147.1, 143.7, 142.2, 142.1, 140.6, 139.7, 139.6, 138.5, 137.3, 136.9, 135.0, 134.3, 133.8, 128.7, 128.0, 127.7, 125.2, 124.5, 124.0, 123.6, 121.3, 119.5, 119.1, 117.3, 114.8, 68.4, 63.1, 62.9, 35.6, 31.7, 31.5, 31.3, 31.2, 30.2, 29.7, 29.1, 22.6, 14.1. HRMS (MALDI) *m/z*: M⁺, calcd for C₁₅₂H₁₅₂N₄O₂S₄, 2194.0832; found, 2193.334.

Synthesis of IDT-CHO. The procedure is similar to that of IDTIDT-CHO. The crude compound was purified by silica gel column using a mixture of hexane/DCM as the eluent to give a yellow solid (530 mg, 65%). ¹H NMR (400 MHz, CDCl₃, δ): 9.82 (s, 2H), 7.65 (s, 2H), 7.58 (s, 2H), 7.13 (m, 16H), 2.57 (t, *J* = 8.0 Hz, 8H), 1.60–1.53 (m, 8H), 1.35–1.29 (m, 24H), 0.86 (t, *J* = 4.0 Hz, 12H). ¹³C NMR (125 MHz, CDCl₃, δ): 182.4, 156.5, 154.7, 149.9, 145.9, 141.7, 140.1, 135.4, 131.5, 128.2, 127.2, 118.7, 62.3, 35.1, 31.2, 30.8, 28.6, 22.1, 13.7. HRMS (MALDI) *m/z*: M⁺, calcd for C₆₆H₇₄O₂S₂, 962.5130; found, 962.180.

Synthesis of IDT-IC. 1,1-Dicyanamethylene-3-indanone (194 mg, 1.0 mmol) was added into the mixture of compound IDT-CHO (95 mg, 0.1 mmol) in chloroform with pyridine (1 mL), the reactant was deoxygenated with nitrogen for 30 min and then refluxed for 10 h. After cooling to room temperature, the reaction was poured into methanol and the precipitate was filtered off. It was then extracted with DCM and washed with water. The crude product was purified by silica gel column using a mixture of hexane/DCM as the eluent to give a purple solid (106 mg, 81%). ¹H NMR (400 MHz, CDCl₃, δ): 8.90 (s, 2H), 8.70 (d, *J* = 8.0 Hz, 2H), 7.92 (d, *J* = 8.0 Hz, 2H), 7.77 (m, 8H), 7.14 (m, 16H), 2.60 (t, *J* = 8.0 Hz, 8H), 1.60–1.53 (m, 8H), 1.30 (m, 24H), 0.87 (t, *J* = 4.0 Hz, 12H). HRMS (MALDI) *m/z*: M⁺, calcd for C₉₀H₈₂N₄O₂S₂, 1314.5879; found, 1314.740.

Device fabrication

The PSCs were fabricated in the configuration of ITO/PEDOT:PSS/PTB7-Th : IDTIDT-IC or PTB7-Th : IDT-IC (1 : 1.5, w/w)//PDINO/Al. ITO-coated glass substrates (CSG Holding Co., Ltd, 10 ohm sq^{−1}) were cleaned sequentially with deionized water, acetone, ethanol, and isopropanol under sonication for 10 min each and then treated with oxygen plasma for 15 min to

generate the hydrophilic surface. The filtered PEDOT:PSS solution (Clevious P VP AI 4083) was spin-coated onto the cleaned ITO substrates at 3000 rpm for 50 s, followed by baking at 150 °C for 20 min in air. Subsequently, the substrates were transferred into a N₂-filled glove box for spin-coating of the photoactive layer. PTB7-Th (1-Material Chemscitech Inc., St-Laurent, Quebec, Canada) and non-fullerene acceptor (IDTIDT-IC and IDT-IC) were dissolved in *o*-dichlorobenzene with a donor/acceptor weight ratio of 1 : 1.5. The mixed solution was spin-coated on top of the PEDOT:PSS layer at 1500 rpm for 90 s, followed by thermal annealing at 150 °C for 10 min. Methanol solution of PDINO with a concentration of 0.5 mg mL⁻¹ was then spin-coated on the photoactive layer at 3000 rpm for 30 s. Finally, Al top electrode was deposited onto the PDINO buffer layer by thermal evaporation at a base pressure of 1.0 × 10⁻⁴ Pa. The deposition rate and film thickness were monitored with a quartz crystal sensor. A shadow mask was put on the sample to define an active area of 4 mm² before the Al deposition.

Device characterization

The current density–voltage (*J*–*V*) characteristics were measured using a Keithley 2400 source meter unit under simulated Air Mass 1.5 Global (AM 1.5 G) solar illumination at an intensity of 100 mW cm⁻², which was calibrated by a reference silicon solar cell. The measurements were carried out with the OPVs inside the glove box (<0.1 ppm O₂ and H₂O). The incident photon-to-current conversion efficiency (IPCE) was measured by a solar cell spectral response measurement system (Enli Technology Co., Ltd., QE-R3011). The light intensity was calibrated using a single-crystal Si photovoltaic cell as a standard.

SCLC mobility measurements. Electron-only devices with a configuration of ITO/cesium carbonate (Cs₂CO₃)/PTB7-Th:IDTIDT-IC or PTB7-Th:IDT-IC/Ca/Al was fabricated to examine the electron mobilities of blend films. Cs₂CO₃ (0.2 wt%), dissolved in 2-ethoxyethanol, was spin-coated on ITO substrate at 3000 rpm and then baked at 150 °C for 20 min. After active layer spin-coating, 16 nm of Ca and 80 nm of Al were thermally deposited onto the photoactive layer. The electron mobilities were determined by fitting the dark current to the space-charge-limited current (SCLC) model that includes field-dependent mobility, given by

$$J = \frac{9}{8} \varepsilon_r \varepsilon_0 \mu_0 \frac{V_{\text{eff}}^2}{L^3} \exp\left(\beta \sqrt{\frac{V_{\text{eff}}}{L}}\right) \quad (2)$$

where ε_0 is the vacuum permittivity, ε_r is the relative dielectric constant of the active layer, μ_0 is the zero-field mobility, V_{eff} is the effective voltage which is determined by subtracting the built-in voltage from the applied voltage, L is the thickness of the active layer, and β is the field-activation factor.

FTPS measurements. The modulated illumination beam of a Bruker Vertex 70 FTIR with an external detector option was used. For the scaling to absolute EQE_{PV}, a calibrated silicon photodiode was used as a reference detector.

Acknowledgements

This work was supported by the National Natural Science Foundation of China (21504062, 21202114, 21204054, 51303118, 91333204), the Natural Science Foundation of Jiangsu Province (BK20130289), China Postdoctoral Science Foundation Funded Project (2015M581853), Jiangsu Province Postdoctoral Science Foundation Funded Project (1501024B), The Priority Academic Program Development of Jiangsu Higher Education Institutions, Programs Foundation of the Ministry of Education of China (20133201120008), A Project Funded by the Priority Academic Program Development of Jiangsu Higher Education Institutions, the Beijing National Laboratory for Molecular Sciences (20140112), and State and Local Joint Engineering Laboratory for Novel Functional Polymeric Materials. Yuxin Xia was funded by the CSC graduate student stipend ship, FG acknowledges the Open Research Fund of State Key Lab of Silicon Materials (Zhejiang University) and OI acknowledges support from the Knut and Alice Wallenberg foundation through a Wallenberg Scholar grant, as well as funding from the Science Council, Sweden.

Notes and references

- 1 Y. Liu, J. Zhao, Z. Li, C. Mu, W. Ma, H. Hu, K. Jiang, H. Lin, H. Ade and H. Yan, *Nat. Commun.*, 2014, **5**, 5293.
- 2 Z. He, B. Xiao, F. Liu, H. Wu, Y. Yang, S. Xiao, C. Wang, T. P. Russell and Y. Cao, *Nat. Photonics*, 2015, **9**, 174.
- 3 (a) W. Li, K. H. Hendriks, A. Furlan, M. M. Wienk and R. A. J. Janssen, *J. Am. Chem. Soc.*, 2015, **137**, 2231; (b) K. Gao, L. Li, T. Lai, L. Xiao, Y. Huang, F. Huang, J. Peng, Y. Cao, F. Liu, T. P. Russell, R. A. J. Janssen and X. Peng, *J. Am. Chem. Soc.*, 2015, **137**, 7282; (c) M. Wang, H. Wang, T. Yokoyama, X. Liu, Y. Huang, Y. Zhang, T.-Q. Nguyen, S. Aramaki and G. C. Bazan, *J. Am. Chem. Soc.*, 2014, **136**, 12576.
- 4 J. Yao, T. Kirchartz, M. S. Vezie, M. A. Faist, W. Gong, Z. He, H. Wu, J. Troughton, T. Watson, D. Bryant and J. Nelson, *Phys. Rev. Appl.*, 2015, **4**, 014020.
- 5 W. Shockley and H. J. Queisser, *J. Appl. Phys.*, 1961, **32**, 510.
- 6 K. Vandewal, K. Tvingstedt, A. Gadisa, O. Inganäs and J. V. Manca, *Nat. Mater.*, 2009, **8**, 904.
- 7 W. Tress, N. Marinova, O. Inganäs, M. K. Nazeeruddin, S. M. Zakeeruddin and M. Graetzel, *Adv. Energy Mater.*, 2015, **5**, DOI: 10.1002/aenm.201400812.
- 8 (a) Y. Zhong, M. T. Trinh, R. Chen, W. Wang, P. P. Khlyabich, B. Kumar, Q. Xu, C. Y. Nam, M. Y. Sfeir, C. Black, M. L. Steigerwald, Y. L. Loo, S. Xiao, F. Ng, X. Y. Zhu and C. Nuckolls, *J. Am. Chem. Soc.*, 2014, **136**, 15215; (b) S. Holliday, R. S. Ashraf, C. B. Nielsen, M. Kirkus, J. A. Röhr, C.-H. Tan, E. Collado-Fregoso, A.-C. Knall, J. R. Durrant, J. Nelson and I. McCulloch, *J. Am. Chem. Soc.*, 2015, **137**, 898; (c) J. W. Jung, J. W. Jo, C.-C. Chueh, F. Liu, W. H. Jo, T. P. Russell and A. K. Y. Jen, *Adv. Mater.*, 2015, **27**, 3310; (d) Y. Liu, C. Mu, K. Jiang, J. Zhao, Y. Li, L. Zhang, Z. Li, J. Y. Lai, H. Hu, T. Ma, R. Hu, D. Yu, X. Huang, B. Z. Tang and H. Yan, *Adv. Mater.*, 2015, **27**,

- 1015; (e) Y. Zang, C.-Z. Li, C.-C. Chueh, S. T. Williams, W. Jiang, Z.-H. Wang, J.-S. Yu and A. K. Y. Jen, *Adv. Mater.*, 2014, **26**, 5708; (f) D. Sun, D. Meng, Y. Cai, B. Fan, Y. Li, W. Jiang, L. Huo, Y. Sun and Z. Wang, *J. Am. Chem. Soc.*, 2015, **137**, 11156; (g) Y. Liu, C. Mu, K. Jiang, J. Zhao, Y. Li, L. Zhang, Z. Li, J. Y. L. Lai, H. Hu, T. Ma, R. Hu, D. Yu, X. Huang, B. Z. Tang and H. Yan, *Adv. Mater.*, 2015, **27**, 1015; (h) H. Li, Y. J. Hwang, B. A. Courtright, F. N. Eberle, S. Subramanian and S. A. Jenekhe, *Adv. Mater.*, 2015, **27**, 3266; (i) J. Zhao, Y. Li, H. Lin, Y. Liu, K. Jiang, C. Mu, T. Ma, J. Y. Lin Lai, H. Hu, D. Yu and H. Yan, *Energy Environ. Sci.*, 2015, **8**, 520; (j) Y. Lin, J. Wang, Z.-G. Zhang, H. Bai, Y. Li, D. Zhu and X. Zhan, *Adv. Mater.*, 2015, **27**, 1170; (k) Y. Lin, Z.-G. Zhang, H. Bai, J. Wang, Y. Yao, Y. Li, D. Zhu and X. Zhan, *Energy Environ. Sci.*, 2015, **8**, 610; (l) Y. Lin and X. Zhan, *Mater. Horiz.*, 2014, **1**, 470; (m) D. Meng, D. Sun, C. Zhong, T. Liu, B. Fan, L. Huo, Y. Li, W. Jiang, H. Choi and T. Kim, *J. Am. Chem. Soc.*, 2016, **138**, 375; (n) O. K. Kwon, M. A. Uddin, J. H. Park, S. K. Park, T. L. Nguyen, H. Y. Woo and S. Y. Park, *Adv. Mater.*, 2015, DOI: 10.1002/adma.201504091; (o) H. Lin, S. Chen, Z. Li, J. Y. L. Lai, G. Yang, T. McAfee, K. Jiang, Y. Li, Y. Liu and H. Hu, *Adv. Mater.*, 2015, **27**, 7299; (p) S. Li, W. Liu, M. Shi, J. Mai, T.-K. Lau, J. Wan, X. Lu, C.-Z. Li and H. Chen, *Energy Environ. Sci.*, 2016, **9**, 604.
- 9 Y. Li, K. Yao, H.-L. Yip, F.-Z. Ding, Y.-X. Xu, X. Li, Y. Chen and A. K. Y. Jen, *Adv. Funct. Mater.*, 2014, **24**, 3631.
- 10 G. Xing, N. Mathews, S. Sun, S. S. Lim, Y. M. Lam, M. Grätzel, S. Mhaisalkar and T. C. Sum, *Science*, 2013, **342**, 344.
- 11 Z.-G. Zhang, B. Qi, Z. Jin, D. Chi, Z. Qi, Y. Li and J. Wang, *Energy Environ. Sci.*, 2014, **7**, 1966.
- 12 (a) F. Padinger, R. S. Rittberger and N. S. Sariciftci, *Adv. Funct. Mater.*, 2003, **13**, 85; (b) C. Y. Chang, C. E. Wu, S. Y. Chen, C. Cui, Y. J. Cheng, C. S. Hsu, Y. L. Wang and Y. Li, *Angew. Chem., Int. Ed.*, 2011, **50**, 9386; (c) S. C. Price, A. C. Stuart, L. Yang, H. Zhou and W. You, *J. Am. Chem. Soc.*, 2011, **133**, 4625; (d) C. m. Cabanetos, A. El Labban, J. A. Bartelt, J. D. Douglas, W. R. Mateker, J. M. Fréchet, M. D. McGehee and P. M. Beaujuge, *J. Am. Chem. Soc.*, 2013, **135**, 4656; (e) C. Y. Chang, Y. J. Cheng, S. H. Hung, J. S. Wu, W. S. Kao, C. H. Lee and C. S. Hsu, *Adv. Mater.*, 2012, **24**, 549; (f) Y. Liang, Z. Xu, J. Xia, S. T. Tsai, Y. Wu, G. Li, C. Ray and L. Yu, *Adv. Mater.*, 2010, **22**, E135; (g) H. Zhou, L. Yang, A. C. Stuart, S. C. Price, S. Liu and W. You, *Angew. Chem., Int. Ed.*, 2011, **123**, 3051; (h) Y. X. Xu, C. C. Chueh, H. L. Yip, F. Z. Ding, Y. X. Li, C. Z. Li, X. Li, W. C. Chen and A. K. Y. Jen, *Adv. Mater.*, 2012, **24**, 6356; (i) C. M. Amb, S. Chen, K. R. Graham, J. Subbiah, C. E. Small, F. So and J. R. Reynolds, *J. Am. Chem. Soc.*, 2011, **133**, 10062; (j) M. Wang, X. Hu, P. Liu, W. Li, X. Gong, F. Huang and Y. Cao, *J. Am. Chem. Soc.*, 2011, **133**, 9638; (k) A. T. Yiu, P. M. Beaujuge, O. P. Lee, C. H. Woo, M. F. Toney and J. M. Fréchet, *J. Am. Chem. Soc.*, 2012, **134**, 2180; (l) Y. Li, J. Zou, H.-L. Yip, C.-Z. Li, Y. Zhang, C.-C. Chueh, J. Intemann, Y. Xu, P.-W. Liang, Y. Chen and A. K. Y. Jen, *Macromolecules*, 2013, **46**, 5497; (m) V. S. Gevaerts, A. Furlan, M. M. Wienk, M. Turbiez and R. A. J. Janssen, *Adv. Mater.*, 2012, **24**, 2130; (n) I. Meager, R. S. Ashraf, S. Mollinger, B. C. Schroeder, H. Bronstein, D. Beatrup, M. S. Vezie, T. Kirchartz, A. Salleo, J. Nelson and I. McCulloch, *J. Am. Chem. Soc.*, 2013, **135**, 11537; (o) J. W. Jung, J. W. Jo, F. Liu, T. P. Russell and W. H. Jo, *Chem. Commun.*, 2012, **48**, 6933; (p) J. W. Jung, F. Liu, T. P. Russell and W. H. Jo, *Energy Environ. Sci.*, 2013, **6**, 3301; (q) Q. Peng, Q. Huang, X. Hou, P. Chang, J. Xu and S. Deng, *Chem. Commun.*, 2012, **48**, 11452; (r) L. Dou, J. Gao, E. Richard, J. You, C.-C. Chen, K. C. Cha, Y. He, G. Li and Y. Yang, *J. Am. Chem. Soc.*, 2012, **134**, 10071; (s) N. Li, D. Baran, K. Forberich, F. Machui, T. Ameri, M. Turbiez, M. Carrasco-Orozco, M. Drees, A. Facchetti and F. C. Krebs, *Energy Environ. Sci.*, 2013, **6**, 3407; (t) V. S. Gevaerts, A. Furlan, M. M. Wienk, M. Turbiez and R. A. Janssen, *Adv. Mater.*, 2012, **24**, 2130; (u) Y.-J. Hwang, B. A. E. Courtright, A. S. Ferreira, S. H. Tolbert and S. A. Jenekhe, *Adv. Mater.*, 2015, **27**, 4578; (v) H. Li, Y.-J. Hwang, B. A. E. Courtright, F. N. Eberle, S. Subramanian and S. A. Jenekhe, *Adv. Mater.*, 2015, **27**, 3266.
- 13 (a) Z. Tang, B. Liu, A. Melianas, J. Bergqvist, W. Tress, Q. Bao, D. Qian, O. Inganäs and F. Zhang, *Adv. Mater.*, 2015, **27**, 1900; (b) D. B. Sulas, K. Yao, J. J. Intemann, S. T. Williams, C.-Z. Li, C.-C. Chueh, J. J. Richards, Y. Xi, L. D. Pozzo and C. W. Schlenker, *Chem. Mater.*, 2015, **27**, 6583.
- 14 C. Schwarz, H. Bässler, I. Bauer, J.-M. Koenen, E. Preis, U. Scherf and A. Köhler, *Adv. Mater.*, 2012, **24**, 922.
- 15 A. A. Bakulin, A. Rao, V. G. Pavelyev, P. H. van Loosdrecht, M. S. Pshenichnikov, D. Niedzialek, J. Cornil, D. Beljonne and R. H. Friend, *Science*, 2012, **335**, 1340.
- 16 Y. Zhang, S.-C. Chien, K.-S. Chen, H.-L. Yip, Y. Sun, J. A. Davies, F.-C. Chen and A. K. Y. Jen, *Chem. Commun.*, 2011, **47**, 11026.